# One step synthesis of niobium doped titania nanotube arrays to form (N,Nb) co-doped TiO 2 with high visible light photoelectrochemical activity

Thomas Cottineau, Nicolas Béalu, Pierre-Alexandre Gross, Sergey Pronkin, Nicolas Keller, Elena Savinova, Valérie Keller

Journal Name

Dynamic Article Links ►

Cite this: DOI: 10.1039/c0xx00000x

www.rsc.org/xxxxxx

ARTICLE TYPE

# One step synthesis of niobium doped titanium dioxide nanotube arrays by anodization to form (N,Nb) co-doped $TiO_2$ with an enhanced visible light photoelectrochemical activity†

**Thomas Cottineau,* Nicolas Béalu, Pierre-Alexandre Gross, Sergey N. Pronkin, Nicolas Keller, Elena R. Savinova *and* Valérie Keller.***

***Received (in XXX, XXX) Xth XXXXXXXXX 20XX, Accepted Xth XXXXXXXXX 20XX***
**DOI: 10.1039/b000000x**

The chemical modification of aligned titanium dioxide nanotube ($TiO_2$-NTs) arrays provides new doping possibilities to improve their photoelectrochemical activity under visible light. Niobium doped $TiO_2$-NTs containing up to 15% of Nb in the near-surface region are prepared by a flexible single step procedure using a fluoroniobate complex simultaneously acting as a source of the doping element and fluoride anions required for nanotube formation. This negatively charged complex allows an efficient insertion of Nb in the forming $TiO_2$-NTs structure during the anodization process. These nanotube arrays are further modified with nitrogen to achieve (Nb,N) co-doped nanotubes with noticeable visible light photoelectrochemical activity.

## Introduction

The anodization of metallic titanium to form aligned titanium dioxide nanotube ($TiO_2$-NTs) arrays, first reported by Gong and co-workers,[1] has been studied for over a decade and allows formation of nanotubes with a diameter of approximately 100 nm and a length which can be varied from 100 nm to 1 mm by controlling the anodization parameters.[2,3,4] These nanostructures have attracted considerable interest due to the wide range of their potential applications. For instance, they can be used in photovoltaic[5,6] or photoelectrochemical[3] cells, taking advantage of an essentially unidirectional flow of photogenerated electrons along the nanotube axis in the aligned nanostructure and a reduced charge carrier recombination at intergranular boundaries when compared to a film consisting of $TiO_2$ nanoparticles.[7] Due to the high surface to volume ratio offered by these structures, $TiO_2$-NTs are also promising for sensing applications for detection of various chemicals including explosives.[8,9,10] Recently, aligned $TiO_2$-NTs were obtained on foreign substrates (FTO, Si, graphene) by a two step method consisting in the deposition of a metallic titanium layer and its anodization to form nanotubes, offering new possibilities for photovoltaic and photoelectrochemical conversion applications.[5,11,12]

Titanium dioxide is one of the most studied materials for solar to chemical energy conversion applications owing to its high photoactivity, large natural abundance, ease of synthesis at low price, and high (photo-)chemical stability.[3,13,14] Furthermore, for photoelectrochemical water splitting, the position of the $TiO_2$ valence and conduction bands allows both oxygen and hydrogen evolution reactions.[15] However, due to its large band gap (> 3.1 eV), only a small part of the solar spectrum ($\lambda$ < 400 nm) is absorbed and can be efficiently used for the photoconversion.

To this regard, doping of $TiO_2$ to improve visible light absorption is particularly important for photoelectrochemical applications. Two main doping approaches are currently considered for various applications, namely anionic (with N, C, P…),[16,17] and cationic doping (with metal ions).[18,19] Visible light absorption was reported for N doped $TiO_2$ nanoparticles or nanotubes and a small associated photoelectrochemical activity in the visible part of the solar spectrum was measured. Unfortunately, this was accompanied by a strong decrease of the activity in the UV and the overall photoelectrochemical conversion efficiency was strongly reduced.[20] This is explained by the higher recombination rate of the photogenerated charge carriers. Indeed, nitrogen doping induces strongly localised states in the gap of $TiO_2$ that act as trap centers.

Lately, several theoretical[21,22,23] and experimental studies[24,25] have proposed a co-doping approach as an efficient way to reduce the $TiO_2$ band gap and adjust the energy band level in favor of photoelectrochemical reactions. This method combines the cationic doping with metal cations substituting $Ti^{4+}$ in its lattice positions, with the anionic doping. This co-doping approach is believed to improve both the solubility of dopants in the solid semiconductor material, and the stability of the resulting structure by favoring its charge neutrality.[22] The co-doping should also improve the photochemical properties of the material when compared to the monodoping approach, in which the high concentration of dopant needed for band gap reduction led to low quality material with high probability of charge carrier recombination.[21,22] In particular, for the water splitting, 4d and 5d cations with energy levels similar to titanium 3d orbital energy (Nb, Ta, Mo…) can replace Ti in its lattice positions allowing mixing of their d orbitals in the conduction band without

lowering its minimum energy. At the same time the introduction of 2p or 3p anions in the $TiO_2$ structure can raise the valence band maximum energy and then reduce the band gap.[21,24]

In the specific case of $TiO_2$-NTs produced by anodization, different anionic and cationic doping methods have been investigated. Thermal treatments in specific atmospheres containing a precursor of the doping species ($NH_3$, urea, acetylene, CO…) have been successfully employed for the anionic doping with N and C.[26,27] Ion implantation is another method that has proven to be efficient for the nitrogen doping of $TiO_2$-NTs for visible light absorption.[28] It should be noted however that the latter method requires special equipment to achieve useful doping levels and presents a high risk of damaging the nanotubular structure.[29] The cationic modification can be performed by introducing the second metal in the formed nanotubular structure of $TiO_2$-NTs, *e.g.* by immersion of $TiO_2$-NTs in a solution containing a precursor of the metal cation eventually followed by a thermal annealing.[30] The second metal usually forms a separate oxide phase (in the form of nanoparticles), and this method is of interest to form heterojunctions between two semiconductors, *i.e.* $TiO_2$-NTs/NiO,[31] $TiO_2$-NTs/$Fe_3O_4$,[32] with an enhanced visible light response. However, detachment of metal oxide particles from the nanotubular substrate cannot be excluded. Another method for cationic doping of $TiO_2$ nanotubes consists in the anodization of alloys containing both the titanium and the doping metal. By this way, synthesis of organized nanotubular or nanoporous oxide layers has been obtained through anodization of TiAl,[33] TiZr,[34] TiMo,[35] TiNb,[36] TiTa,[37] TiW[38] and TiCu[39] alloys. Depending on the doping metal, this method provides possibilities to form either mixed oxide nanotubes (both metal oxide phase are identified) or doped $TiO_2$-NTs with improved photocatalytic or photoelectrochemical properties.[40] However, this approach requires metal alloy substrates, and the concentration of the dopant in the resulting nanotubular structure is difficult to control. The distribution of the dopant in resulting nanotubes may be inhomogeneous since the solid solution of various metals (Mo, Nb…) in metallic titanium cannot be obtained for a whole range of concentrations.[41,42] Furthermore, achieving this synthesis on foreign substrates like FTO requires a method for the co-deposition of titanium and the alloying metal.[39]

Here we report on the synthesis of niobium doped and niobium nitrogen co-doped $TiO_2$-NTs through a flexible method in which neither special alloy substrates nor elaborated equipment are required. The cationic doping method relies on the use of an ammonium fluoroniobate precursor during the anodization process. This precursor provides niobium atoms but also fluorides necessary for the nanotubular structure formation. By this method, the niobium concentration in the nanotubes can be easily adjusted through the control of the precursor concentration in the electrolyte used during the anodization process. A post synthesis thermal annealing under $NH_3$ atmosphere allows the production of (Nb,N) co-doped $TiO_2$-NTs with a strongly enhanced photoelectrochemical activity for water splitting under visible light. Furthermore, while for the N-doped $TiO_2$-NTs the photoelectrochemical conversion efficiency in the UV part of the spectrum is strongly attenuated by the doping, it remains significant for the co-doped nanotubes.

## Experimental details

### Pristine and doped $TiO_2$-NTs synthesis

Before anodization, titanium foils (MaTeck GmbH; 99.6%) were cleaned in *aqua regia* (1:3 $HNO_3$:HCl) for 3 minutes, rinced with ultrapure water and dried under $N_2$ flux. This treatment was followed by a further cleaning in successive ultrasonic bath of acetone ethanol and finally ultrapure water for 5 minutes each and drying under $N_2$ flux. Titanium dioxide nanotubes were synthesized in ethylene glycol based electrolyte containing 1.0%$_{v/v}$ of ultrapure water and 0.3%$_{w/w}$ of $NH_4F$ (Sigma-Aldrich, 98%).[43] For niobium doped nanotubes, an ammonium fluoroniobate salt was used (Sigma-Aldrich; 99.99%; $(NH_4)_5[(NbOF_4)2(NbF_7)]$). Ammonium fluoroniobate was added to the electrolyte in different proportions but the total fluoride concentration was kept constant at $[F^-]$ = 0.09 mol $L^{-1}$ ($F^-$ from $NH_4F$ + $F^-$ from ammonium fluoroniobate).

The synthesis was conducted in a two electrode cell constituted of a Teflon vessel. A platinum foil was used as counter electrode and a titanium foil as the working electrode. The temperature of the electrolyte was maintained at 25 ± 1 °C by a thermocryostat. The anodization potential was applied using a Biologic SP-300 potentiostat with a 48 V booster module. A 1000 mV $s^{-1}$ potential ramp was applied to the Ti foils from open circuit potential until potential reached 45 V. The potential was maintained at 45 V until the charge transferred during the synthesis reaches 4.0 C $cm^{-2}$. The electrode was rinsed immediately after the synthesis with ultra pure water, to avoid nanotubes dissolution, and dried by $N_2$ stream.

The obtained nanotubes electrodes were annealed either under a 100 cc $min^{-1}$ air or $NH_3$ flux (pure $NH_3$ or diluted in $N_2$ in a 1/5 proportion). The temperature was increased from room temperature to 550°C with a 2°C $min^{-1}$ ramp. That temperature was maintained for 2 hours, then the heating was stopped and the oven was allowed to cool down.

### Characterization methods

XPS analysis was performed by Multilab 2000 Thermoelectron spectrometer with Al Kα source (λ=1486.6 eV) spectra were analyzed and fitted with CasaXPS software. All spectra were calibrated to the binding energy of adventitious carbon at 285.0 eV. All data were fitted using a Shirley function for the background and Voigt function with a Lorentzian ratio of 30% for the different peaks. All parameters were left free during the fit except the area ratio between the two Ti 2p (and Nb 3d) peaks fixed at 0.5 (and 0.666).

Scanning Electron Microscopy (SEM) images were obtained in secondary electron mode using a JEOL 6700F equipped with a Field Emission Gun with an extraction potential of 2.5 kV. The working distance was set to 5 mm. The dimensions of $TiO_2$-NTs were evaluated from SEM images using statistical analysis of measurements, realized on at least 10 nanotubes per samples, with ImageJ program.

X Ray Diffraction measurements were done in a classical θ/θ configuration using a Bruker D8 Advance diffractometer equipped with a LynxEye PSD detector, using the Cu Kα radiation and operating at 40 kV and 40 mA. The measurements were made using a step of 0.0079° (2θ) and an acquisition time of 4.5 s $step^{-1}$. The different peaks of anatase $TiO_2$, rutile $TiO_2$ and α

Ti were assigned according to the Powder Diffraction Files 01-089-4921, 01-089-8304 and 00-044-1294 respectively. Data analysis was conducted with WinXPOW program to fit the diagrams. The cell parameters refinement was done using Checkcell program. The diffraction peaks of the metallic titanium foil were used as an internal reference.

The conductivities of the different electrolytes were measured with a Metrohm 712 conductometer calibrated with different NaCl solutions at 25°±1 C.

**Photoelectrochemical measurements**

Photoelectrochemical (PEC) measurements were performed in a 3 electrode cell filled with 0.1 mol $L^{-1}$ $H_2SO_4$ with a platinum counter electrode and a Mercury Sulphate Electrode (MSE) as reference. The compartment of the working electrode has a quartz window for illumination of the sample of nanotubes which as a surface of 0.28 $cm^2$ delimited by an O-ring. The light source is an Oriel 200 W EmArc passing through a Cornerstone 130 monochromator. The entrance and exit slits of the monochromator are set to obtain a resolution of 5 nm. The photocourant density $j_p(\lambda)$ is measured with a Biologic SP-300 potentiostat for an applied potential of +0.2 V vs MSE. The power density arriving on the cell $P(\lambda)$ is controlled in real-time by a powermeter (918D Newport) placed behind a beam sampler used to collect a part of the beam heading to the cell. EQE is measured between 280 and 800 nm with a step of 5 nm.

## Results and discussion

### Niobium doped $TiO_2$-NTs

**Electrochemical synthesis**

In the present study, the synthesis of pristine titanium dioxide nanotubes is performed in an ethylene glycol based electrolyte. The anodization mechanism can be schematically described as a competition between the electrochemical oxidation of titanium into $TiO_2$ and the field-assisted dissolution of the oxide by the fluoride according to equations 1 and 2, respectively.[2,4]

$$Ti + 2\,H_2O \rightarrow TiO_2 + 4\,e^- + 4\,H^+ \quad (1)$$

$$TiO_2 + 6\,F^- + 4\,H^+ \rightarrow [TiF_6]^{2-} + 2\,H_2O \quad (2)$$

To obtain niobium modified nanotubes, the anodization is performed in the presence of ammonium fluoroniobate salt ($(NH_4)_5[(NbOF_4)2(NbF_7)]$) which is added to the electrolyte (for details see the experimental section). With this precursor, the negatively charged fluoroniobate complexes ($NbF_7^{2-}$ and $NbOF_4^-$) are expected to be driven, under the influence of the electric field, to the titanium anode where $TiO_2$-NTs are being formed. To explore the effect of the doping level on the properties of the resulting material, the ammonium fluoroniobate precursor is added to the electrolyte in different concentrations while keeping the total fluoride concentration ($F^-$ from $NH_4F$ + $F^-$ from ammonium fluoroniobate) constant at $[F^-]$ = 0.09 mol $L^{-1}$. The molar ratio, $x$, between $F^-$ originating from $(NH_4)_5[(NbOF_4)2(NbF_7)]$ and the total fluoride concentration is $x$ = 0, 0.25, 0.5, 0.75 and 1. Thus, when $x$ = 0, $NH_4F$ is the only source of fluoride, while for $x$ = 1 all fluoride originates from the ammonium fluoroniobate precursor. Hereafter, $x$ is referred as the Nb precursor ratio, and the corresponding samples are noted $x$ Nb/$TiO_2$-NTs.

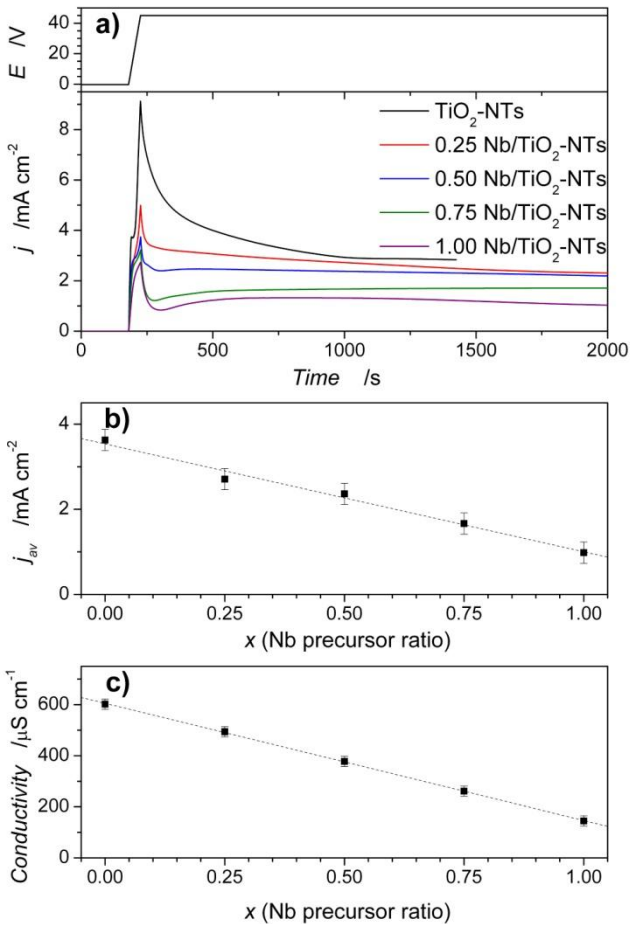


**Fig. 1** a) Applied voltage bias (top) and resulting current transients (bottom) for the anodization of a Ti foil in ethylene glycol containing 1 $\%_{v/v}$ of $H_2O$, and different amounts of $NH_4F$ and fluoroniobate precursor. Evolution of b) the average current and c) the electrolyte conductivity with the niobium precursor ratio $x$.

Current transients for the anodization of different samples are presented in figure 1.a). In order to obtain $TiO_2$ nanotubes with comparable lengths, the anodization was performed until the anodic charge attained the value of 4.0 ± 0.1 C $cm^{-2}$. The current decreases after the potential has reached 45 V and tends to a steady state value under the constant voltage. The charge transferred during the anodization process divided by the anodization time, hereafter referred as an average anodization current $j_{av}$, is presented in figure 1.b) for different samples. As the ratio $x$ of fluoroniobate precursor increases from 0 to 1, the average current decreases following a linear trend from 3.6 to 1.0 ± 0.2 mA $cm^{-2}$. This increase of $x$ is accompanied by a diminution of the measured electrolyte conductivity from 600 to 150 ± 10 µS $cm^{-1}$ (figure 1.c) suggesting decrease of the fluoride concentration due to its coordination to $Nb^{5+}$. A similar decrease of the current density with the fluoride concentration has been observed for $TiO_2$-NTs anodized in an ethylene glycol based electrolyte.[44,45]

**SEM electrodes characterizations**

In all cases, anodization leads to the formation of nanotubular structures as it can be seen from scanning electron microscopy (SEM) images presented in figure 2 for three samples obtained in electrolytes with different contents of niobium precursor. The

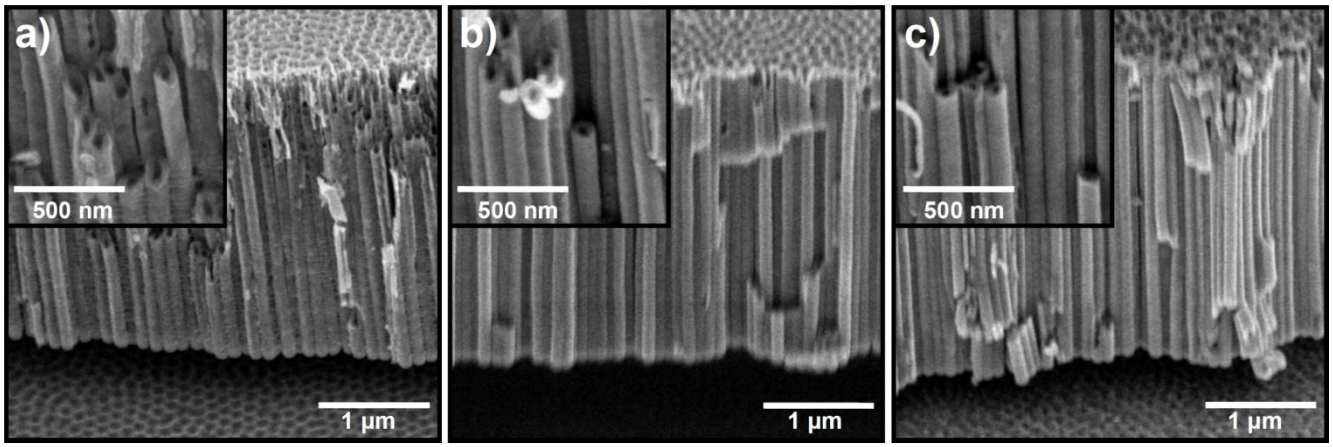


**Fig. 2** SEM images at 45° inclined view of: a) $TiO_2$-NTs; b) 0.5 Nb/$TiO_2$-NTs and c) 1.0 Nb/$TiO_2$-NTs. The insets show magnifications of the nanotubular structure.

doped and undoped nanotubes synthesized under these conditions have internal and external diameters of 50 ± 10 and 110 ± 10 nm, respectively, and a typical length of 3500 ± 300 nm.

One can notice that the nanotubular structure is formed even when ammonium fluoronobiate is the only source of fluoride (figure 2.c) suggesting the presence of some amount of uncoordinated fluoride in the electrolyte. The latter can be produced by a partial hydrolysis of the fluoroniobate and/or oxofluoroniobate complexes according to equations 3 and 4 respectively:

$$NbF_7^{2-} + H_2O \rightleftarrows NbOF_4^- + 2\,H^+ + 3\,F^- \quad (3)$$

$$NbOF_4^- + H_2O \rightleftarrows NbO_2F + 2\,H^+ + 3\,F^- \quad (4)$$

The presence of uncoordinated fluoride in the electrolyte is necessary for the dissolution of the oxide passive layer located at the interface with metallic titanium (eq. 2) and the formation of the nanotubular structure.[2,4]

**XPS measurements**

X ray-photoelectron spectroscopy (XPS) experiments were conducted for different samples to obtain information on the nanotube surface composition. Survey spectra of $TiO_2$-NTs and 1.0 Nb/$TiO_2$-NTs are presented in figure 3.a). Besides the peaks of titanium, carbon and oxygen, the contributions of niobium appear clearly in the survey spectrum of niobium modified $TiO_2$-NTs. Figure 3.b) shows the Nb 3d spectra for the samples obtained in electrolytes with different niobium precursor ratios *x*. The position of the $3d_{5/2}$ peak at 207.7 ± 0.1 eV and the $3d_{5/2}/3d_{3/2}$ doublet separation energy of 2.8 ± 0.1 eV are in agreement with the values reported for $Nb^{5+}$ (in $Nb_2O_5$ for instance[46]) and no supplementary contributions are observed. A strong decrease of the peak intensity is observed when *x* is reduced.

O 1s and Ti 2p spectra are presented in figure 3.c) and d) respectively. The main contribution of oxygen located at 530.6 ± 0.1 eV is attributed to oxygen in $TiO_2$ crystal lattice. The second contribution (532.3 ± 0.1 eV) is attributed to hydroxyl groups that are present at the nanotube surface. This contribution can also reflect the presence of oxygen from carboxyl and alcohol groups from contamination adsorbed at the $TiO_2$ surface that cannot be excluded.[47] For titanium the position of the $2p_{3/2}$ peak (459.2 ± 0.1 eV) and the doublet separation energy (5.7 ± 0.1 eV) are typical of $Ti^{4+}$ in titanium dioxide. The niobium doping does not affect either the number or the position of Ti, O and C peaks, but changes the relative intensities of Nb and Ti peaks.

The evolution of the surface atomic percentage of niobium calculated as Nb/(Nb+Ti) with the niobium precursor ratio, *x*, is presented in figure 3.e). An increase of *x* from 0.25 to 1.0 results in an exponential raise of the Nb content which attains 15 ± 0.1 % of the cationic content with ammonium fluoroniobate being the only source of fluoride. For comparison, a sample of pristine $TiO_2$-NTs was synthesized, rinsed, dried under $N_2$ flux and then immersed for 60 minutes in the electrolyte where $NH_4F$ was fully substituted by ammonium fluoroniobate precursor but without applying any voltage. For this sample, XPS experiment indicates that less than 0.1 ± 0.1 % of niobium is present at the surface. This observation suggests that the insertion of fluoroniobate complex is driven by the positive electric field.

Comparison between the bulk and the surface composition of niobium doped nanotubes points out to inhomogeneity of the Nb concentration across the nanotube wall thickness. Indeed, for the 1.0 Nb/$TiO_2$-NTs sample with the surface atomic concentration of 15% Nb, the bulk concentration (determined by Energy Dispersive X-ray analysis coupled with Transmission Electronic Microscopy) was only 4% (see in Supplementary Information). The incorporation of large anions such as phosphate, oxalate and chromate in porous anodic aluminium oxide was already reported with noticeable anion concentrations. The insertion occurs via adsorption and electric field driven transport across the growing oxide layer and can lead to inhomogeneous distribution of the ionic species in the film.[48]

We infer that the negative charge on the Nb complex is essential for its insertion in $TiO_2$. If this assertion is right, an addition of water should decrease the Nb doping level, since hydrolysis results in the formation of less charged or even neutral fluoroniobate complexes. In order to verify this, the anodization of the titanium foil was performed in an electrolyte containing $5\%_{v/v}$ instead of $1\%_{v/v}$ of $H_2O$ and ammonium fluoroniobate precursor being the only fluoride source (all other anodization parameters were identical). Indeed, while SEM images (presented in Supplementary Information) confirmed the formation of

Cite this: DOI: 10.1039/c0xx00000x

www.rsc.org/xxxxxx

ARTICLE TYPE

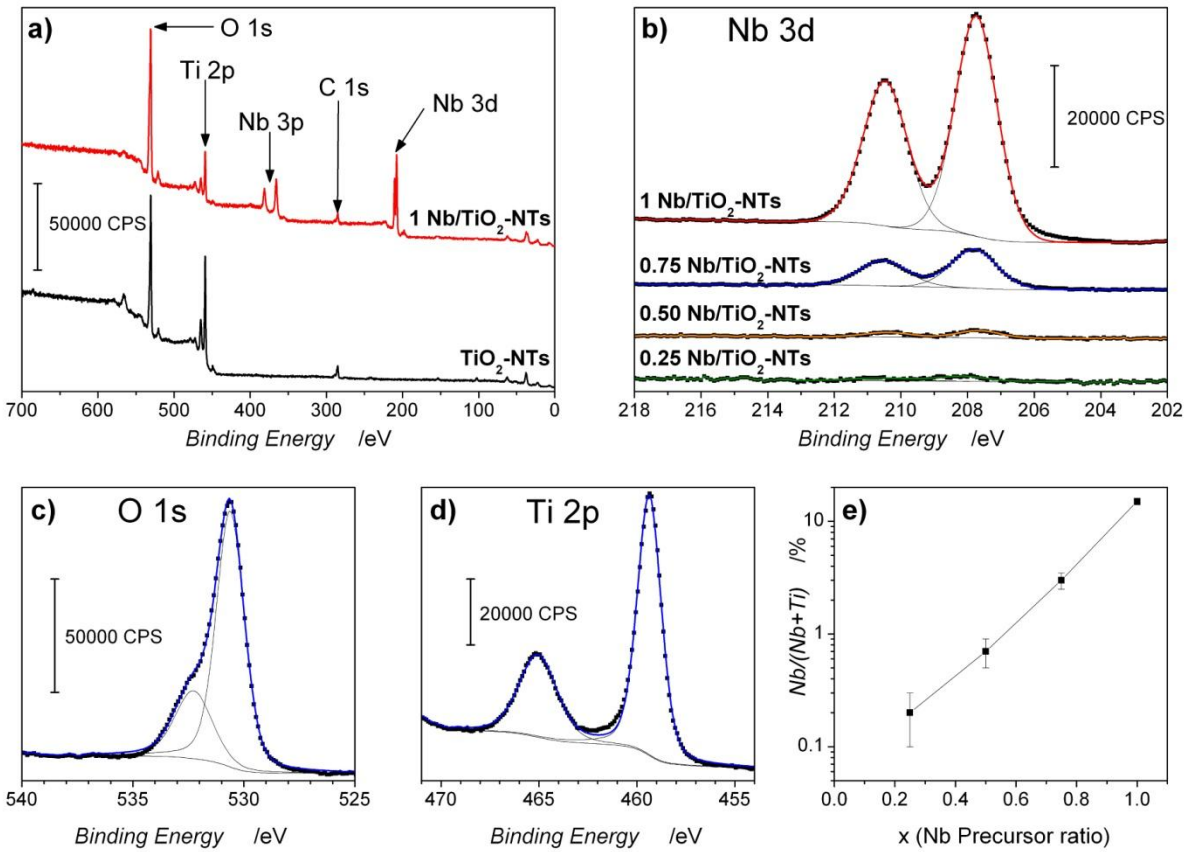


**Fig. 3** a) XPS survey spectra of $TiO_2$-NTs and 1.0 Nb/$TiO_2$-NTs; b) Nb 3d spectra for $TiO_2$-NTs modified with different *x* ratio; Typical spectra of c) O 1s and d) Ti 2p; Black squares are the experimental data and bold lines are the fitted results. e) evolution of the Nb/(Nb+Ti) ratio in regard to the *x* niobium precursor ratio within the electrolyte.

nanotubes with comparable characteristic dimensions, the XPS analysis showed the niobium content of only 2 ± 0.1% against 15 ± 0.1% for the sample anodized in the electrolyte with 1%$_{v/v}$ of $H_2O$. This is in agreement with the electric field driven insertion of an anionic Nb complex into the $TiO_2$ and confirms the combined influence of both water and fluoroniobate precursor contents in the electrolyte on the final concentration of niobium in the nanotubes.

**Nitrogen doping of nanotube arrays**

After anodization, the $TiO_2$ and niobium doped $TiO_2$ nanotubes are amorphous, an annealing of the samples is then required to transform them into crystalline anatase or rutile $TiO_2$-NTs. The thermal treatment is done for 2 h at 550°C either in (i) air, or (ii) pure ammonia, or (iii) diluted ammonia (20% $NH_3$/80% $N_2$). The samples are hereafter noted /air, /p.$NH_3$ and /d.$NH_3$, respectively. The objective of $NH_3$ annealing is to produce N doped $TiO_2$-NTs and (N,Nb) co-doped $TiO_2$-NTs.

**XRD measurements**

For all samples, whatever the thermal treatment atmosphere used, X-ray diffraction diagrams presented in figure 4, indicate the presence of anatase and a small content of rutile as expected for nanotubes annealed at this temperature.[2,4] The sharp peaks are attributed to the α phase of metallic titanium from the substrate. For niobium doped nanotubes, no phase of niobium oxide has been detected even for highly doped nanotubes. For samples annealed in ammonia no phase of niobium or titanium oxynitride or nitride are visible in XRD patterns. It can be seen that annealing under $NH_3$ flux changes the relative intensity of the different anatase peaks: when annealed in air, the (101) reflexion at 25.28° is the more intense whereas for samples annealed in ammonia the (004) peak at 37.80° is the more intense. This traduces a change in the orientation of the crystallite for the nanotubes annealed in ammonia or the change in the structure factor due to the presence of nitrogen atoms.

The different diagrams were fitted and the positions of the peaks were indexed using the reflections of metallic titanium as an internal reference. With this data, the lattice parameters of anatase of the different samples are calculated and gathered in

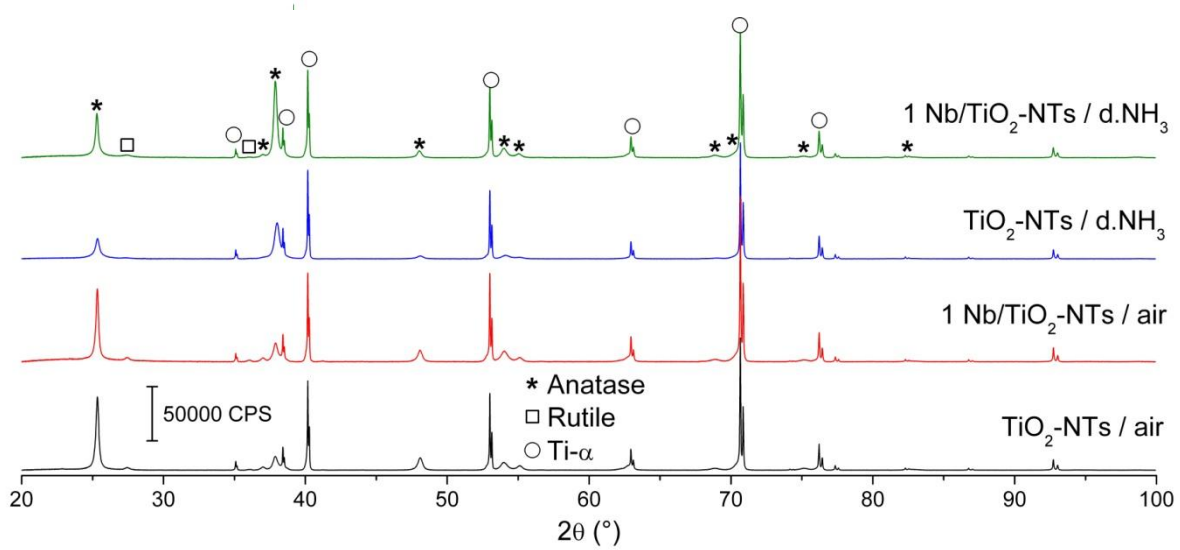


**Fig. 4** DRX diagrams for $TiO_2$-NTs and 1 Nb/$TiO_2$-NTs samples annealed in air or $NH_3$. The main peaks of anatase, rutile and titanium α are identified by stars, squares and circles, respectively. The peaks were attributed using the corresponding PDF files.

**Table 1** Lattice parameters of anatase for the different samples. The Δ values are calculated using $TiO_2$-NTs sample as reference.

| Sample | a [Å] | c [Å] | V [Å$^3$] | Δa[%] | Δc[%] | ΔV[%] |
|---|---|---|---|---|---|---|
| $TiO_2$-NTs air | 3.7844(7) | 9.5003(6) | 136.06(5) | - | - | - |
| 1 Nb/$TiO_2$-NTs air | 3.7856(5) | 9.5033(7) | 136.19(3) | 0.03 | 0.03 | 0.09 |
| $TiO_2$-NTs d.$NH_3$ | 3.7908(9) | 9.4941(7) | 136.43(8) | 0.17 | -0.01 | 0.27 |
| 1 Nb/$TiO_2$-NTs d.$NH_3$ | 3.7942(8) | 9.4955(6) | 136.70(5) | 0.26 | -0.05 | 0.47 |

table 1. The addition of niobium leads to slightly increased lattice parameters of anatase $TiO_2$ ($\Delta V_{cell}$ = +0.10 ± 0.03%) that confirms the substitution of titanium by niobium cations. A greater extension of the lattice parameters is observed for $TiO_2$-NTs annealed in $NH_3$ atmosphere ($\Delta V_{cell}$ = +0.27 ± 0.03%) suggesting an efficient nitrogen insertion. This effect is enhanced when niobium doped nanotubes are annealed in $NH_3$ ($\Delta V_{cell}$ = +0.47 ± 0.03%) suggesting that nitrogen insertion is enhanced in the presence of niobium. The latter can be explained by the need to compensate the excess positive charge induced by the substitution of $Ti^{4+}$ by $Nb^{5+}$. For niobium doped $TiO_2$ annealed in air, the charge compensation can be explained by three phenomena: the presence of titanium vacancies, the introduction of interstitial oxygen or the presence of free electrons that can reduce $Ti^{4+}$ to $Ti^{3+}$.[24] It should be noted that no peak of $Ti^{3+}$ was observed by XPS in our samples, excluding a significant formation of $Ti^{3+}$.

**XPS analysis**

The influence of the annealing in air or pure ammonia atmosphere for undoped and niobium doped titanium dioxide nanotubes, was studied by XPS, and the corresponding N 1s spectra are shown in figure 5. It should be noted that niobium doped $TiO_2$-NTs samples annealed under $NH_3$ have a niobium concentration similar to that of amorphous samples or samples annealed under air. For $TiO_2$-NTs annealed in air, two contributions of nitrogen are observed, located at 399.8 ± 0.2 eV and 401.8 ± 0.2 eV. These contributions are generally assigned to

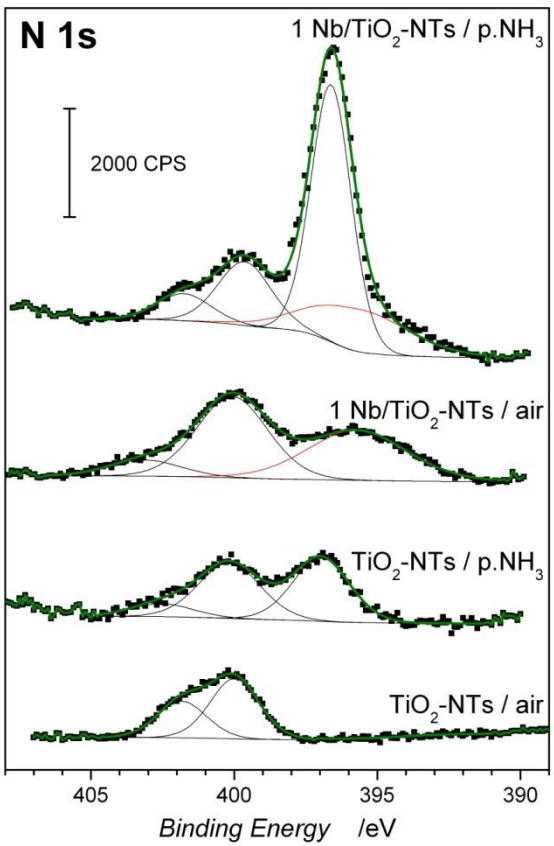


**Fig. 5** N 1s XPS spectra for $TiO_2$-NTs and 1 Nb/$TiO_2$-NTs after thermal treatments at 550°C in air or in pure $NH_3$ for 2 h. Black squares are the experimental data, bold lines are the fitted results and red lines correspond to the Nb 3p satellite peaks.

adsorbed nitrogen, γ-$N_2$, or nitrogen atoms from organic compounds adsorbed on the $TiO_2$ surface.[49,50] Two similar contributions are observed for niobium doped nanotubes annealed

Cite this: DOI: 10.1039/c0xx00000x

www.rsc.org/xxxxxx

ARTICLE TYPE

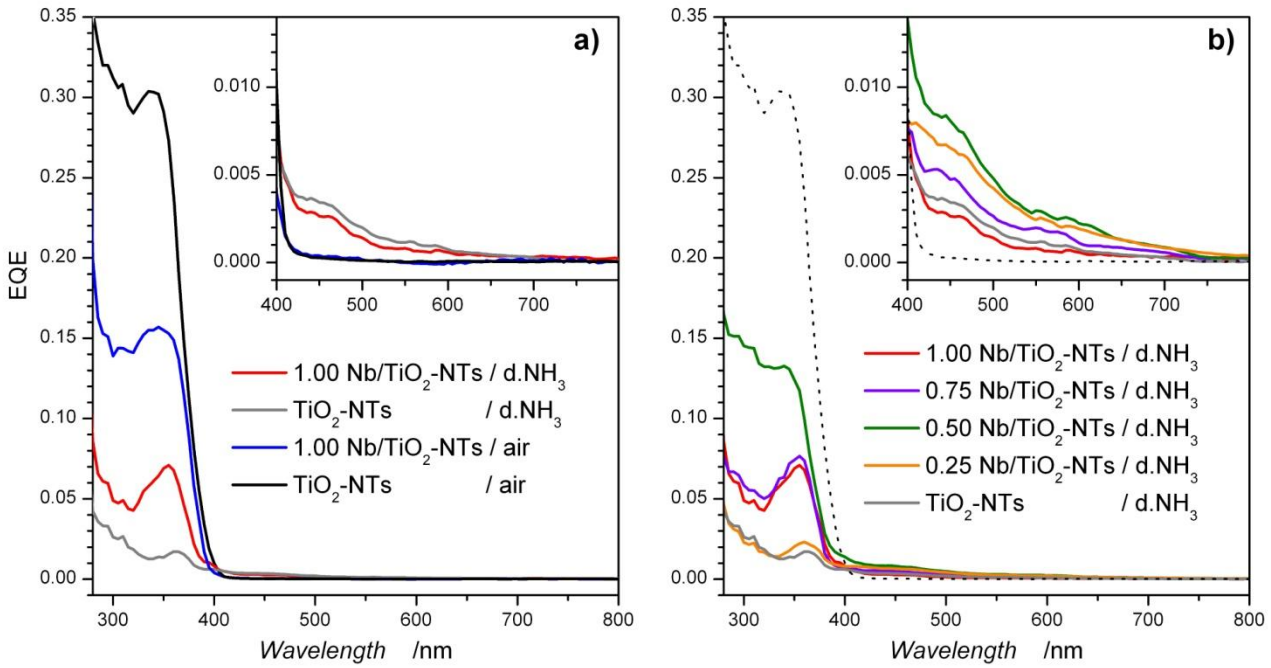


**Fig. 6** External Quantum Efficiency (EQE) in 0.1 mol $L^{-1}$ $H_2SO_4$ and applied potential of +0.2 V vs MSE for a) $TiO_2$-NTs, N-, Nb- and (N,Nb)-doped $TiO_2$-NTs. Inset is an enlargement of the EQE in the visible spectral region. b) EQE for (N,Nb) co-doped $TiO_2$-NTs with different content of niobium annealed in $NH_3$. The dotted line corresponds to the $TiO_2$-NTs sample annealed in air.

in air. In this case, the full width at half maximum (FWHM) of these peaks is increased by 50% when compared to the sample without niobium. The broadening of these peaks may be explained by the overlap of several contributions of nitrogen species adsorbed on Ti or Nb oxide surface sites with slightly different binding energies. The present signal/noise ratio of N1s spectra is not sufficient for a clear identification of these different contributions. A third broad peak appears at 395.7 ± 0.2 eV corresponding to the Nb 3p satellite (indicated by red lines on figure 5).[51]

When annealed in ammonia flux, the N 1s spectra of both $TiO_2$-NTs and 1.0 Nb/$TiO_2$-NTs samples exhibit a supplementary peak at 396.7 ± 0.2 eV. This value, typical of atomic β-N, is observed in titanium nitride or N-doped $TiO_2$ obtained by sputtering methods in nitrogen environments.[16] For 1.0 Nb/$TiO_2$-NTs annealed in pure $NH_3$, the β-N peak has a higher intensity. For $TiO_2$-NTs annealed in pure ammonia flux, β-N peak represents 39% of the total nitrogen, whereas for Nb-doped nanotubes this ratio increases to 68%. The ratio between β-N and metallic cations present at the surface (Ti + Nb in the case of Nb-doped nanotubes) increases from 1.4% for N doped $TiO_2$-NTs to 6.9% for (N,Nb) co-doped nanotubes. Nitrogen doping with $NH_3$ is thus strongly increased in the presence of niobium in the structure. A possible explanation for the enhanced nitrogen content in niobium doped $TiO_2$-NTs annealed in ammonia can be a reduced energy of formation of the co-doped $TiO_2$ crystalline structure when compared to the N or Nb mono-doped $TiO_2$, as suggested by first principle calculations for (N,Ta) and (N,W) co-doped $TiO_2$.[22,23] For (N,Nb) co-doped $TiO_2$-NTs, the ratio between β-N and Nb is 0.46, thus the positive charge induced by Nb is only partially compensated by nitrogen at the surface of nanotubes.

UV/visible absorption spectra of the different samples are presented in supplementary information (Fig. S4). A shift of the absorption toward lower energies is clearly observed for N-doped and (N,Nb) co-doped $TiO_2$-NTs samples.

**Photoelectrochemical measurements**

The influence of the N-doping, Nb-doping or (N,Nb) co-doping on the photoelectrochemical response of $TiO_2$-NTs samples is tested in a water splitting experiment. Measurements are conducted in a 3 electrode cell with a mercury sulfate electrode (MSE) as reference, in 0.1 mol $L^{-1}$ $H_2SO_4$. The nanotube electrode is the photoanode and a platinum counter electrode is the cathode for oxygen and hydrogen evolution reactions, respectively (eq. 5 and 6).

$$2\ h^+ + H_2O \rightarrow 1/2\ O_2 + 2\ H^+ \quad (5)$$

$$2\ H^+ + 2\ e^- \rightarrow H_2 \quad (6)$$

It should be noted that samples annealed under pure $NH_3$ flux, are almost inactive for photoelectrochemical measurements. This

is probably due to a too high concentration of nitrogen atoms which would not only participate to a reduction of the bandgap, but also can act as recombination centers.[16] Furthermore, for this annealing condition, Nb 3d XPS spectra (presented in Supplementary Information) indicate the presence of a supplementary contribution characteristic of niobium oxynitride or suboxide.[52] The presence of these new phases at the surface can be also responsible for the lower activity of these samples. Therefore, the photoelectrochemical experiments are conducted for N-doped samples obtained by annealing in a flow of ammonia diluted in nitrogen (XPS spectra for these samples are given in Supplementary Information.).

In figure 6 are presented the External Quantum Efficiency (*EQE*) results that can be defined as the ratio between the number of collected electrons and the number of incident photons on the cell according to equation 7:

$$EQE(\lambda) = \frac{h \cdot c}{e}\left(\frac{j_p(\lambda)}{P(\lambda)\lambda}\right) \quad (7)$$

$j_p(\lambda)$ and $P(\lambda)$ are the measured photocurrent and the incident light power density at a given wavelength λ, respectively.

Undoped and Nb-doped $TiO_2$-NTs annealed in air, show photoelectrochemical activity in UV light (λ < 400 nm) with the maximum conversion efficiency around 30 and 15%, respectively (figure 6.a). For Nb doped nanotubes the absorption edge is slightly shifted toward the smaller wavelength as expected from the slightly higher bandgap value of niobium oxide compared to $TiO_2$.[53] For $TiO_2$-NTs sample annealed in diluted ammonia atmosphere, the UV light absorption is decreased to less than 3%, which can be explained by the presence of strongly localized N 2p states in the band gap that tend to trap on empty states the photogenerated charge carriers.[22] This decrease of the activity was already reported for N doped $TiO_2$ nanoparticles and nanotubes.[20] In the case of 1.0 Nb/$TiO_2$-NTs annealed in the same conditions, the absorption in the UV part of spectra is less reduced (EQE = 7%). This confirms the positive effect of niobium which reduces the charge recombination due to nitrogen doping of $TiO_2$. Based on first principles calculations this positive effect of Nb can be explained by the presence of continuum-like hybridized states from N 2p and Nb 4d orbitals above the valence band instead of the localized states appearing for N-doped $TiO_2$.[22] A closer look at the EQE in the visible part of the spectrum (λ > 400 nm; inset of figure 6.a) indicates that absorption of light is strongly enhanced in the presence of nitrogen. For $TiO_2$-NTs and 1.0 Nb/$TiO_2$-NTs annealed in diluted $NH_3$, a visible light photoelectrochemical activity is observed and the EQE in the visible increases up to 0.5% at 400 nm.

For (Nb,N) co-doped $TiO_2$-NTs, the photoconversion efficiency is studied against the niobium content, controlled by the ratio *x* of the niobium precursor in the anodization electrolyte (figure 6.b). The overall conversion yields, normalized for an AM1.5 reference spectrum (American Society Testing and Materials G173-03 Global tilt), are calculated for different spectral domains: UV (280 < λ < 400 nm), visible (400 < λ < 800 nm) and for the whole AM1.5 spectrum (280 < λ < 4000 nm) according to:[54]

**Table 2** Calculated yields for the different samples in the UV, visible and whole spectral domain (AM1.5) for undoped and Nb-doped $TiO_2$-NTs samples annealed in air or diluted $NH_3$.

| Sample | Annealing gaz | Yield[a] | UV Yield[b] | Vis Yield[c] |
|---|---|---|---|---|
| $TiO_2$-NTs | air | 0.115(5) | 2.439(8) | 0.004(5) |
| 1 Nb/$TiO_2$-NTs | air | 0.086(5) | 1.800(8) | 0.005(5) |
| $TiO_2$-NTs | d.$NH_3$ | 0.032(5) | 0.261(8) | 0.038(5) |
| 0.25 Nb/$TiO_2$-NTs | d.$NH_3$ | 0.055(5) | 0.309(8) | 0.075(5) |
| 0.50 Nb/$TiO_2$-NTs | d.$NH_3$ | 0.117(5) | 1.488(8) | 0.090(5) |
| 0.75 Nb/$TiO_2$-NTs | d.$NH_3$ | 0.067(5) | 0.835(8) | 0.052(5) |
| 1.00 Nb/$TiO_2$-NTs | d.$NH_3$ | 0.054(5) | 0.828(8) | 0.030(5) |

[a] % / whole solar spectrum (280> λ > 4000 nm).

[b] % / λ < 400 nm.

[c] % / 800> λ > 400 nm.

$$\eta = \frac{e}{h \cdot c}\left(V^0_{rev} - V_{bias}\right)\left(\frac{\int_{\lambda_{min}}^{\lambda_{max}} EQE(\lambda) P(\lambda) d\lambda}{P_t}\right) \quad (8)$$

With $P_t$ the total irradiation power density for the considered spectral domain, *i.e.* 1000.4, 46.1, 543.0 W $m^{-2}$ for the complete, UV and visible spectral domain respectively. $V^0_{rev}$ is the standard reversible potential for the water splitting reaction (1.229 V) and $V_{bias}$ the applied potential during the measurement of EQE, *i.e.* the difference between the applied potential and the open circuit potential of the electrode under irradiation. The complete analysis of the conversion efficiency for different samples in different spectral intervals (UV, visible and whole AM1.5 spectrum) is presented in table 2. It appears that both visible and UV light photoelectrochemical conversion show an optimum for 0.5 Nb/$TiO_2$-NTs. In this case, EQE in UV is similar to that observed for 1.0 Nb/$TiO_2$-NTs annealed in air and the visible light EQE reaches1.4% at 400 nm. Even if this value seems not very high, it is 3 times greater than values reported for N-doped $TiO_2$ nanoparticles,[55] N-doped $TiO_2$ nanotubes[56] or N doped niobium oxide (≈ 0.4% at 400 nm in all cases).[57] The positive effect of the (N,Nb) co-doping can be emphasized by comparing $TiO_2$-NTs and 0.5 Nb/$TiO_2$-NTs annealed in diluted ammonia: for co-doped samples, the visible light conversion yield is more than 2 times greater and in UV light region (λ > 400 nm), the conversion efficiency is 5 times greater when compared to N-doped $TiO_2$-NTs. The comparison between $TiO_2$-NTs annealed in air and0.5 Nb/$TiO_2$-NTs annealed in diluted ammonia indicates visible light (λ > 400 nm) conversion efficiency 20 times greater for the sample annealed in $NH_3$.

## Conclusions

In summary, we have developed a new method to incorporate niobium in aligned $TiO_2$-NTs directly during the anodization step by using a fluoroniobate complex. The niobium concentration in nanotubes can be controlled over a wide range by varying the concentration of the niobium precursor and water in the electrolyte. Furthermore, the ammonium fluoroniobate precursor can be used as the only source of fluorides required for nanotube formation, instead of commonly used HF, KF, or $NH_4F$. We inferred that the presence of the negatively charged fluoroniobate

complex is required to introduce niobium cations in the $TiO_2$ nanotubes growing during the anodization process. This method can be used to dope aligned $TiO_2$-NTs without requiring any special alloys. One can also imagine using this one step synthesis to grow metal doped $TiO_2$-NTs on foreign substrates, like FTO, without using a co-sputtering method for deposition of metallic titanium and a doping element before anodization.

The Nb-doped $TiO_2$-NTs were annealed under ammonia atmosphere to induce cationic/anionic co-doping of $TiO_2$. The nitrogen incorporation in the structure is more efficient when Nb is already present in the $TiO_2$ nanotube structure. The co-doped material exhibits strongly enhanced photoelectrochemical conversion efficiency in the visible light range when comparing to Nb- or N-doped $TiO_2$-NTs, supporting previously published theoretical studies.[21,22] At the same time, the photoelectrochemical conversion properties of co-doped $TiO_2$-NTs are strongly enhanced compared to N-doped nanotubes in the UV part of the spectra.

Even if an optimum composition is determined in this set of data, it appears that the behavior of co-doped systems is quite complex. Supplementary experiments will be conducted to optimize both the niobium and the nitrogen contents for co-doped $TiO_2$-NTs in order to improve their photoelectrochemical efficiency. This doping method will be applied to other fluorometallates to realize titanium dioxide nanotubes doped with other transition metals. The complex electronic structure of these novel anionic/cationic co-doped $TiO_2$-NTs will be studied by defect density and trap energy measurements (temperature dependant photoluminescence, Electrochemical Impedance Spectroscopy). For a better understanding of the structure formation, the cationic doping mechanism and the distribution of the doping elements will also be studied.

## Acknowledgements

The authors are grateful to their colleagues of LMSPC involved in the present work, namely P.Bernhardt (XPS measurements), T. Romero (SEM measurements). Dr. Spiros Zafeiratos and Filipp Napolsky are acknowledged for the fruitful discussions concerning XPS and DRX experiments.

This work was financially supported by CNRS PIE program (PR09-4.1.1-4) and OSEO in the frame of Conectus Alsace Network (A1005007 A-FM).

## Notes and references

*Laboratoire des Matériaux Surface et Procédés pour la Catalyse (LMSPC) UMR 7515 CNRS/Université de Strasbourg.*
*25 rue Becquerel, 67087 Strasbourg (France)*
*Fax: (+33) 03 68 85 27 61; Tel: (+33) 03 68 85 27 38;*
*E-mail: cottineau@unistra.fr, vkeller@unistra.fr*

† Electronic Supplementary Information (ESI) available: Supplementary SEM images, UV/visible absorption of the samples, XPS and EDX results. See DOI: 10.1039/b000000x/

1 D. Gong, C. A. Grimes, O. K. Varghese, W. Hu. R. S. Singh, Z. Chen and E. C. Dickey, *J. Mater. Res*. 2001, **16**, 3331.
2 M. Paulose, H. E. Prakasam, O. K. Varghese, L. Peng, K. C. Popat, G. K. Mor, T. A. Desai and C. A. Grimes, *J. Phys. Chem. C* 2007, **111**, 14992.
3 G. K. Mor and C. A. Grimes, *$TiO_2$ Nanotube Arrays: Synthesis, Properties and Applications*, Springer Science, New York, 2009.
4 P. Roy, S. Berger and P. Schmuki, *Angew. Chem. Int. Ed*. 2011, **50**, 2904.
5 O. K. Varghese, M. Paulose and C. A. Grimes, *Nat. Nanotechnol.* 2009, **4**, 592.
6 P. Chen, J. Brillet, H. Bala, P. Wang, S. M. Zakeerudin and M. Grätzel, *J. Mat. Chem.* 2009, **19**, 5325.
7 G. K. Mor, K. Shankar, M. Paulose, O. K. Varghese and C. A. Grimes, *Nano Lett.* 2006, **6**, 215.
8 G. K. Mor, O. K. Varghese, M. Paulose, K. G. Ong and C. A. Grimes, *Thin Solid Films* 2006, **496**, 42.
9 S. Banerjee, S. K. Mohapatra, M. Misra and I. B. Mishra, *Nanotechnology*, 2009, **20**, 075502.
10 D. Spitzer, T. Cottineau, N. Piazzon, S. Josset, F. Schnell, S. N. Pronkin, E. R. Savinova and V. Keller, *Angew. Chem. Int. Ed*. 2012, **51**, 5334.
11 Y. D. Premchand, T. Djenizian, F. Vacandio and P. Knauth, *Electrochem. Comm.* 2006, **8**, 1840.
12 T. Cottineau, A. Albrecht, I. Janowska, N. Macher, D. Begin, M. J. Ledoux, S. N. Pronkin, E. R. Savinova, N. Keller, V. Keller and C. Pham-Huu, *Chem. Comm*. 2012, **48**, 1224.
13 A. Fujishima and K. Honda, *Nature* 1972, **238**, 37.
14 X. Chen and S. S. Mao, *Chem. Rev*. 2007, **107**, 2891.
15 M. G. Walter, E. L. Warren, J. R. McKone, S. W. Boettcher, Q. Mi, E. A. Santori and N. S. Lewis, *Chem. Rev*. 2010, **110**, 6446.
16 R. Asahi, T. Morikawa, T. Ohwaki, K. Aoki and Y. Taga, *Science* 2001, **293**, 269.
17 K. Shankar, K. C. Tep, G. K. Mor and C. A. Grimes, *J. Phys. D* 2006, **36**, 2361
18 Y.-C. Nah, I. Paramasivam and P. Schmuki, *ChemPhysChem*. 2010, **11**, 2698.
19 A. E. R. Mohamed and S. Rohani, *Energy Environ. Sci*. 2011, **4**, 1065.
20 S. Rani, S. C. Roy, M. Paulose, O. K. Varghese, G. K. Mor, S. Kim, S. Yoriya, T. J. LaTempa and C. A. Grimes, *Phys. Chem. Chem. Phys.* 2010, **12**, 2780.
21 W.-J. Yin, H. Tang, S.-H. Wei, M. M. Al-Jassim, J. Turner and Y. Yan, *Phys. Rev. B* 2010, **82**, 045106.
22 R. Long and N. J. English, *Chem. Phys. Lett*. 2009, **478**, 175.
23 R. Long and N. J. English, *Appl. Phys. Lett*. 2009, **94**, 132102.
24 T. M. Breault and B. M. Bartlett, *J. Phys. Chem. C* 2012, **116**, 5986.
25 H. Liu, G. Liu and X. Shi, *Colloids and Surf. A* 2010, **363**, 35.
26 R. P. Vitiello, J. M. Macak, A. Ghicov, H. Tsuchiya, L. F. P. Dick and P. Schmuki, *Electrochem. Commun.* 2006, **8**, 544.
27 J.-H. Park, S. Kim and A. J. Bard, *Nano Lett.* 2006, **6**, 24.
28 A. Ghicov, J. M. Macak, H. Tsuchiya, J. Kunze, V. Haeublein, L. Frey and P. Schmuki, *Nano Lett.* 2006, **6**, 1080.
29 A. Ghicov, J. M. Macak, H. Tsuchiya, J. Kunze, V. Haeublein and P. Schmuki, *Chem. Phys. Lett.* 2006, **419**, 426.
30 J. Gong, W. Pu, C. Yang and J. Zhang, *Electrochim. Acta* 2012, **68**, 178.
31 N. K. Shrestha, M. Yang, Y.-C. Nah, I. Paramasivam and P. Schmuki, *Electrochem. Commun.* 2010, **12**,. 254.
32 N. K. Shrestha, J. M. Macak, F. Schmidt-Stein, R. Hahn, C. T. Mierke, B. Fabry and P. Schmuki, *Angew. Chem. Int. Ed*. 2009, **48**, 969.
33 S. Berger, H. Tsuchiya and P. Schmuki, *Chem. Mater*. 2008, **20**, 3245.
34 K. Yasuda and P. Schmuki, *Electrochim. Acta* 2007, **52**, 4053.
35 N. K. Shrestha, Y.-C. Nah, H. Tsuchiya and P. Schmuki, *Chem. Commun.* 2009, **15**, 2008.
36 A. Ghicov, M. Yamamoto and P. Schmuki, *Angew. Chem. Int. Ed.* 2008, **120**, 8052.
37 H. Tsuchiya, T. Akaki, J. Nakata, D. Terada, N. Tsuji, Y. Minamino, P. Schmuki and S. Fujimoto, *Corros. Sci.* 2009, **51**, 1528.
38 Y.-C. Nah, A. Ghicov, D. Kim, S. Berger and P. Schmuki, *J. Am. Chem. Soc*. 2008, **130**, 16154.

39 G. K. Mor, O. K. Varghese, R. H. T. Wilke, S. Sharma, K. Shankar, T. J. Latempa, K. S. Choi and C. A. Grimes, *Nano Lett.* 2008, **8**, 1906.
40 Y. Yang, K. Lee, Y. Kado and P. Schmuki, *Electrochem. Commun*. 2012, **17**, 56.
41 J. L. Murray, *Bull. Alloy Phase Diagrams* 1981, **2**, 185.
42 J. L. Murray, *Bull. Alloy Phase Diagrams* 1981, **2**, 55.
43 M. Paulose, K. Shankar, S. Yoriya, H. E. Prakasam, O. K. Varghese, G. K. Mor, T. J. Latempa, A. Fitzgerald and C. A. Grimes, *J. Phys. Chem. B* 2006, **110**, 16179.
44 C. A. Grimes, *J. Mater. Chem*. 2007, **17**, 1451.
45 S. P. Albu, A. Ghicov, J. M. Macak and P. Schmuki, *P. Phys. Stat. Sol. (RRL)* 2007, **1**, R65.
46 E. E. Latta and M. Ronay, *Phys. Rev. Lett.* 1984, **53**, 1984.
47 Y.-F. Gao, Y. Masuda and K. Koumoto, *Langmuir* 2004, **20**, 3188.
48 G. D. Sulka, in *Highly ordered Anodic porous alumina formation by self-organized anodization*, in *Nanostructured Materials in Electrochemistry* (Eftekhari A. Ed.), John Wiley & Sons, 2008.
49 N. C. Saha and H. G. Tompkins, *J. Appl. Phys.* 1992, **72**, 3072.
50 T. Sano, N. Negishi, K. Koike, K. Takeuchi and S. Matsuzawa, *J. Mater. Chem.* 2004, **14**, 380.
51 S. K. Sen, J. Riga and J. Verbist, *Chem. Phys. Lett*. 1976, **39**, 560.
52 A. Darlinski and J. Halbritter, *Surf. Interface Anal.* 1987, **10**, 223.
53 A. Le Viet, M. V. Reddy, R. Jose, B. V. R. Chowdari and S. Ramakrishna, *J. Phys. Chem. C* 2010, **114**, 664.
54 A. B. Murphy, P. R. F. Barnes, L. K. Randeniya, I. C. Plumb, I. E. Grey, M. D. Horne and J. A. Glasscock, *Int. J. Hydrogen Energy* 2006, **31**, 1999.
55 R. Nakamura, T. Tanaka and Y. Nakato, *J. Phys. Chem*. 2004, **108**, 10617.
56 J. M. Macak, A. Ghicov, R. Hahn, H. Tsuchiya and P. Schmuki, *J. Mater. Res.* 2006, **21**, 2824.
57 T. Ruff, R. Hahn, M. S. Killian, H. Asoh, S. Ono and P. Schmuki, *Electrochim. Acta* 2012, **62**, 402.